Chemistry
A European
Journal

Chemistry Europe
European Chemical Societies Publishing

Accepted Article

Title: Synthesis, Mechanism Elucidation and Biological Insights of Tellurium(IV)-containing Heterocycles

Authors: Leandro Piovan, João Pedro A. Souza, Pamela T. Bandeira, Leociley R. A. Menezes, Mateus B. Bespalhok, Débora B. Scariot, Francielle P. Garcia, Siddhartha O. K. Giese, David L. Hughes, Celso V. Nakamura, Andersson Barison, Alfredo R. M. Oliveira, and Renan B. Campos

To be cited as: *Chem. Eur. J.* 10.1002/chem.202102287

Link to VoR: https://doi.org/10.1002/chem.202102287

WILEY-VCH

10.1002/chem.202102287

WILEY-VCH

RESEARCH ARTICLE

Synthesis, Mechanism Elucidation and Biological Insights of Tellurium(IV)-Containing Heterocycles

João Pedro A. Souza,[a] Leociley R. A. Menezes,[a] Francielle P. Garcia,[b] Débora B. Scariot,[b] Pamela T. Bandeira,[a] Mateus B. Bespalhok,[a] Siddhartha O. K. Giese,[a] David L. Hughes,[c] Celso V. Nakamura,[b] Andersson Barison,[a] Alfredo R. M. Oliveira,[a] Renan B. Campos,*[d] and Leandro Piovan*[a]

[a] J. P. A. Souza, Dr. P. T. Bandeira, Dr. L. R. A. Menezes, M. B. Bespalhok, Dr. S. O. K. Giese, Prof. Dr. A. Barison, Prof. Dr. A. R. M. Oliveira, Prof. Dr. L. Piovan
Department of Chemistry, Universidade Federal do Paraná, Curitiba-PR, 81.931-480, Brazil
E-mail: lpiovan@ufpr.br
[b] Dr. D. B. Scariot, Dr. F. P. Garcia, Prof. Dr C. V. Nakamura
Health Sciences Center, Universidade Estadual de Maringá, Maringá-PR, 87.020-900, Brazil
[c] Dr. D. L. Hughes
School of Chemistry, University of East Anglia, Norwich NR4 7TJ, United Kingdom
[d] Prof. Dr. R. B. Campos
Academic Department of Chemistry and Biology, Universidade Tecnológica Federal do Paraná, Curitiba-PR, 81.280-340, Brazil
E-mail: renan@utfpr.edu.br

Supporting information for this article is given via a link at the end of the document.

Abstract: Inspired by the synthetic and biological potential of organotellurium substances, we describe here the synthesis and characterization of a series of five- and six-membered ring organotelluranes containing a Te–O bond. Theoretical calculations elucidated the mechanism for the oxidation-cyclization processes involved in the formation of the heterocycles, consistent with chlorine transfer to hydroxy telluride, followed by cyclization step with simultaneous formation of the new Te–O bond and the OH group deprotonation. Moreover, theoretical calculations also indicated *anti*-diastereoisomers as major products for two-chirality center-containing compounds. Antileishmanial assays against *Leishmania amazonensis* promastigotes disclosed 1,2λ^4-oxatellurane **LQ50** (IC_{50} = 4.1±1.0; SI = 12), 1,2λ^4-oxatellurolane **LQ04** (IC_{50} = 7.0±1.3; SI = 7) and 1,2λ^4-benzoxatellurole **LQ56** (IC_{50} = 5.7±0.3; SI = 6) as more powerful and more selective compounds, up to four times more active than the reference. Stability study supported by ^{125}Te NMR analyses showed that these heterocycles do not suffer structural modifications in aqueous-organic media and up to 65 °C.

Introduction

Tellurium is the only natural chalcogen with no apparent role in vital biological processes. Tellurium toxicity for humans still remains poorly understood, as its biological role is probably less known than metals like osmium and ruthenium.[1] Some of the few reports address the use of tellurium for the synthesis of amino acids and proteins in fungi and bacteria.[2] Despite the presence of tellurium in living organisms occurring only in exceptional cases, synthetic tellurium-containing compounds have been applied in biological systems[3] and reported as promising antioxidant agents,[4] immunomodulator,[5] antimicrobial,[6] anti-inflammatory,[7] antitumoral[8] and enzymatic inhibitors.[9] Additionally, this element has been used for several applications in organic and inorganic chemistry, like materials and medicinal fields.[1,10]

As well established, tetra- and hexa-valent tellurium-containing compounds (Te(IV) and Te(VI)) are exceptions to the Lewis octet rule,[11] being classified as hypervalent compounds.[12] Such hypervalent derivatives present great potential for biological purposes.[13] For decades, numerous studies revealed that the inorganic tellurane **AS101** (Figure 1) is a potent inhibitor of the cysteine proteases such as papain and cathepsin B.[9a,14] From then on, several organic and inorganic hypervalent tellurium compounds were reported as successful enzyme inhibitors, including cysteine,[6g, 9b-c, 15] and threonine proteases (20S proteasome),[9h] and tyrosine phosphatases (PTP1B and YopH),[9f] also indicated as promising antioxidants,[4d] antimicrobial[6c,e, 16] and antitumor agents.[8j]

Another important example of a biologically active tellurium-containing compound is the organotellurane **RT-01** (Figure 1), which presented *in vivo* antiprotozoal activity against *Leishmania amazonensis*, leading to significant decrease of the parasitic load compared to that of the reference drug.[17] Another organotellurane, **RF07** (Figure 1), was described as a powerful leishmanicidal agent for *Leishmania chagasi* amastigotes with selectivity index (SI = CC_{50}/IC_{50}) of 10, relating the specificity of the activity in comparison to the cytotoxicity of the evaluated compound.[18] This compound was previously described as a cysteine protease cathepsin B inhibitor,[9b] and its antileishmanial activity has been associated with inhibition of this enzyme in *L. chagasi* protozoa. It is worth mentioning that the inorganic tellurane **AS101** (Figure 1) also presented antileishmanial activity, with IC_{50} = 26.9 μmol L^{-1} for *Leishmania donovani* promastigotes.[14f]

10.1002/chem.202102287

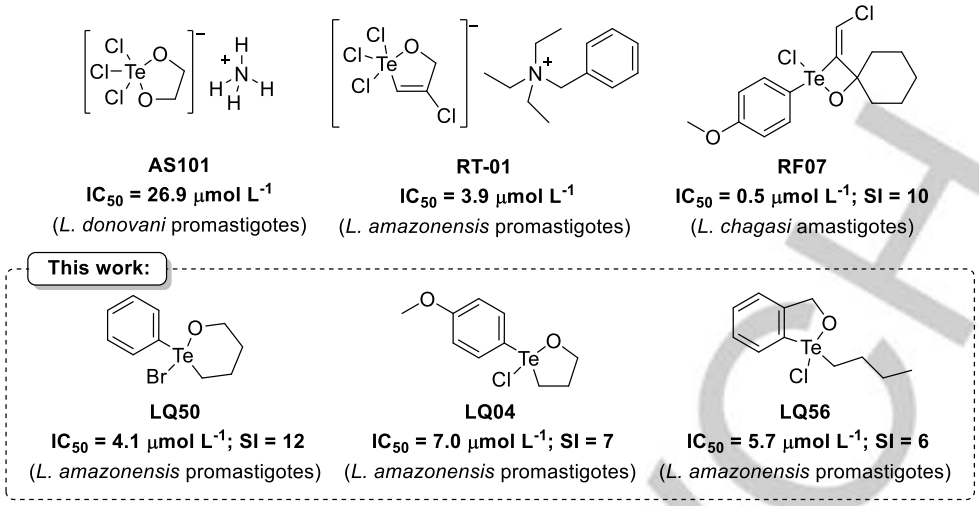

Figure 1. Chemical structures and antileishmanial activities of hypervalent tellurium compounds.

Hypervalent five- and six-membered Te–O bond-containing heterocycles have already been described in the literature;[19] however, their biological properties remain poorly explored. Then, inspired by the potential of hypervalent tellurium compounds, in the current work we discuss: i) the synthesis of a series of five- (1,2λ^4-oxatellurolanes and 1,2λ^4-benzoxatelluroles) and six- (1,2λ^4-oxatelluranes) membered ring organotelluranes; ii) calculations using Density Functional Theory (DFT), performed to identify the most favorable mechanism and to rationalize the diastereoselectivity observed for two-chirality center-containing compounds; iii) the *in vitro* antileishmanial potential of all hypervalent Te(IV)-containing compounds, evaluated against *L. amazonensis* promastigotes; and iv) stability assays supported by ^{125}Te NMR (thermal stability and chemical stability in aqueous-organic media) for some representative hypervalent Te(IV)-containing compounds.

Results and Discussion

Synthesis of Tellurium(IV)-Containing Heterocycles

The synthetic routes to access 1,2λ^4-oxatellurolanes and 1,2λ^4-oxatelluranes were performed as shown in Scheme 1. Bromobenzene (**1a**) or 4-substituted aryl bromides (**1b**-**e**) were reacted with elemental magnesium, followed by the addition of elemental tellurium and later air oxidation, leading to diaryl ditellurides **2a**-**e** in 27-65% isolated yields. The Te–Te bonds from ditellurides **2a**-**e** were cleaved employing sodium borohydride and their respective tellurolates were captured by 3-chloropropan-1-ol to produce hydroxy tellurides **3a**-**e** or by 4-bromobutan-1-ol leading to hydroxy telluride **3f**. Finally, one-pot oxidation-cyclization sequential reactions of **3a-f** employing *N*-chlorosuccinimide (NCS) or *N*-bromosuccinimide (NBS) led to corresponding 1,2λ^4-oxatellurolanes (**LQ02-04**, **33-35** and **48**) in 2-79% isolated yields and 1,2λ^4-oxatelluranes (**LQ49-50**) in 5-15% isolated yields (Scheme 1).

5-Methyl- (**LQ51** and **LQ52**) and 5-phenyl-substituted 1,2λ^4-oxatellurolanes (**LQ53**) were prepared by a 1,4-addition of phenyl tellurolate (from Te–Te bond cleavage of **2a** with $NaBH_4$) to but-3-en-2-one or 1-phenylprop-2-en-1-one, followed by *in situ* carbonyl reduction with $NaBH_4$. In the sequence, NCS or NBS mediated oxidation-cyclization sequential reactions of hydroxy tellurides **3g-h** led to 1,2λ^4-oxatellurolanes **LQ51-53** in 30-79% isolated yields (Scheme 2).

Hydrolysis of the acetal moiety of **3e** led the hydroxy telluro ketone **3i** (90% isolated yield), which was applied as an intermediate for the hydroxy telluro oxime **3j** (82% isolated yield). One-pot sequential oxidation-cyclization sequential using NCS led to the 1,2λ^4-oxatellurolanes **LQ54** and **LQ55** in 30 and 24% isolated yields, respectively (Scheme 3).

2,5-Dihydro-1,2λ^4-benzoxatelluroles **LQ56** and **LQ57** were prepared in 30 and 24% isolated yield, respectively, employing the same oxidation-cyclization approach with NBS or NCS from benzyl hydroxy telluride **3k** (Scheme 4).

All hypervalent Te-containing heterocycles (**LQ02-04**, **LQ33-35** and **LQ48-57**) were purified by precipitation in H_2O/Dimethyl sulfoxide (10:1 v/v) followed by second precipitation in hexane/CH_2Cl_2 (10:1 v/v), and were obtained as odorless white solids with good solubility in organic solvents such as dichloromethane, acetone, tetrahydrofuran, and dimethyl sulfoxide. Eleven chlorinated and five brominated compounds (thirteen unpublished) were obtained in 2−79% isolated yields in the oxidation-cyclization step and overall yields ranging from 0.4% (**LQ35**) to 40% (**LQ52**). Structural characterizations were performed by melting point determination, ^{1}H Nuclear Magnetic Resonance spectroscopy (NMR), ^{13}C NMR, ^{125}Te NMR, Fourier-transform infrared (FTIR) spectroscopy, and single-crystal X-ray diffraction (if applicable).

Structural Characterization by NMR

Rotational restriction and a slightly bent conformation of the five-membered rings in 1,2λ^4-oxatellurolane forced the geminal methylene hydrogens to assume pseudo-axial and pseudo-equatorial positions. Furthermore, tetrasubstituted Te-atom is a chirality center and the methylene hydrogens in the heterocycles are diastereotopic. These structural features are easily observed in three-dimensional projections (Figure 2a, b) and NMR data of representative 1,2λ^4-oxatellurolanes **LQ02** (Figure 2c) and **LQ03** (Figure 2d). Geminal methylene hydrogens presented distinct signals that confirm the heterocyclization as can be seen in correlation maps in Figure 2c and 2d. The multiplicity of hydrogens at position 1 revealed the geminal coupling between them (J = 10.0 Hz) and vicinal couplings with the hydrogens at position 2 (J = 5.8, 4.0 and 3.4 Hz). The same pattern of multiplicity was observed for hydrogens at position 3, with geminal

10.1002/chem.202102287

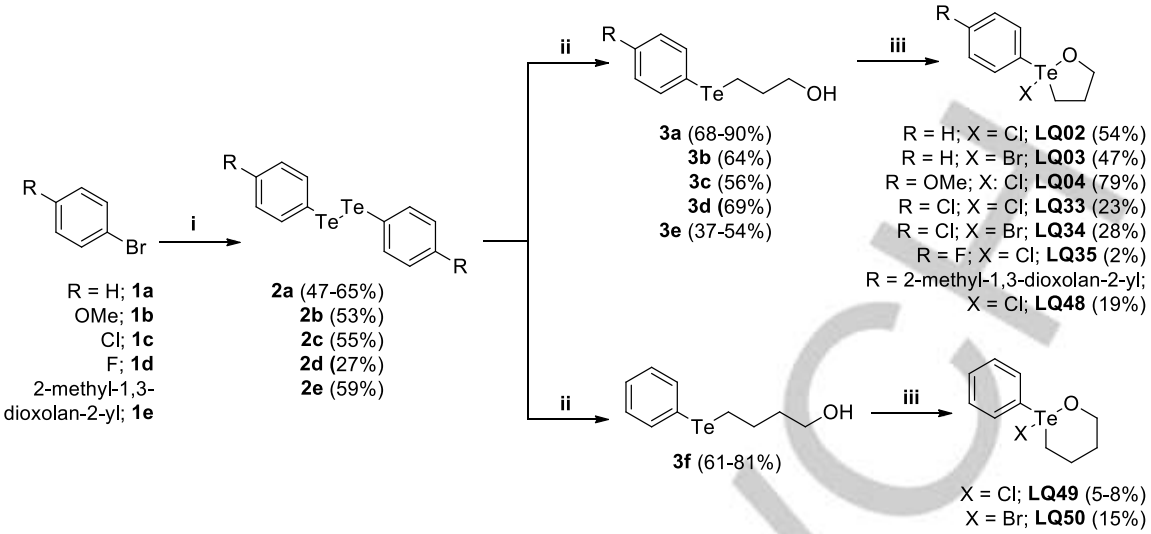

Scheme 1. Synthesis of 1,2λ⁴-oxatellurolanes **LQ02-04**, **33-35** and **48** and 1,2λ⁴-oxatelluranes **LQ49-50**. Reagents and Conditions: i. 1. Mg^0, I_2, tetrahydrofuran, r.t., 2 h; 2. Te^0, 2 h; 3. O_2, 15 min. ii. 3-chloropropan-1-ol or 4-bromobutan-1-ol, $NaBH_4$, H_2O/EtOH, 0 °C-r.t., 1 h. iii. NCS or NBS, CH_2Cl_2, 0 °C-r.t., 30 min.

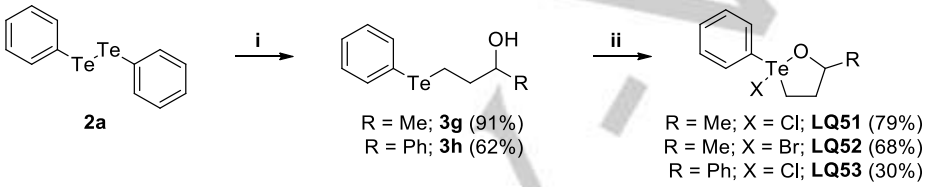

Scheme 2. Synthesis of 1,2λ⁴-oxatellurolanes **LQ51-53**. Reagents and Conditions: i. 1. $NaBH_4$, H_2O/EtOH, 0 °C, 5 min. 2. α,β-unsaturated ketone, 0 °C-r.t., 1 h; 3. $NaBH_4$, 0 °C-r.t., 15 min. ii. NCS or NBS, CH_2Cl_2, 0°C-r.t., 30 min.

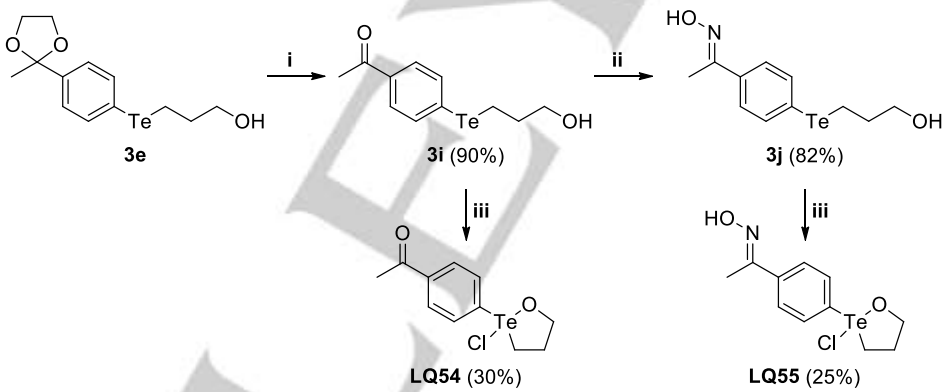

Scheme 3. 2-Methyl-1,3-dioxolan-2-yl group derivatization for the synthesis of 1,2λ⁴-oxatellurolanes **LQ54** and **LQ55**. Reagents and Conditions: i. *p*-toluenesulfonic acid (*p*TSA), acetone, reflux, 2 h. ii. $(NH_3OH)Cl$, AcONa, MeOH, reflux, 2 h. iii. NCS, CH_2Cl_2, 0 °C-r.t., 30 min.

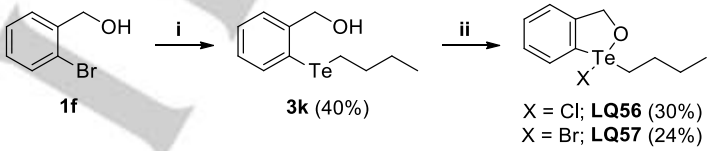

Scheme 4. Synthesis of 1,2λ⁴-benzoxatelluroles (**LQ56** and **LQ57**). Reagents and Conditions: i. 1. BuLi, THF, -78 °C, 30 min; 2. $(BuTe)_2$, r.t., 4 h. ii. NCS or NBS, CH_2Cl_2, 0 °C-r.t., 30 min.

(*J* = 12.1 Hz) and vicinal couplings (*J* = 10.6, 8.2, 7.1 and 3.7 Hz). Thereby, the hydrogens on position 2 showed a complex signal composed by their geminal coupling and four more couplings with close *J* values. The most deshielding hydrogens (at 2.14, 3.70 and 4.75 ppm) occupy pseudo-axial positions for this conformation while the most shielding hydrogens (at 1.90, 3.47 and 3.68 ppm) occupy pseudo-equatorial positions. The chemical shifts, multiplicity, and *J* values for **LQ 02** are detailed in Figure 2e.

$^{13}C\{^1H\}$ NMR spectra comparison of starting material (**3a**) and product (**LQ02**) disclosed significant changes in chemical shifts, mainly for the carbons directly attached to the tellurium atom. Chemical shifts of aliphatic and aromatic carbon atoms (positions

10.1002/chem.202102287

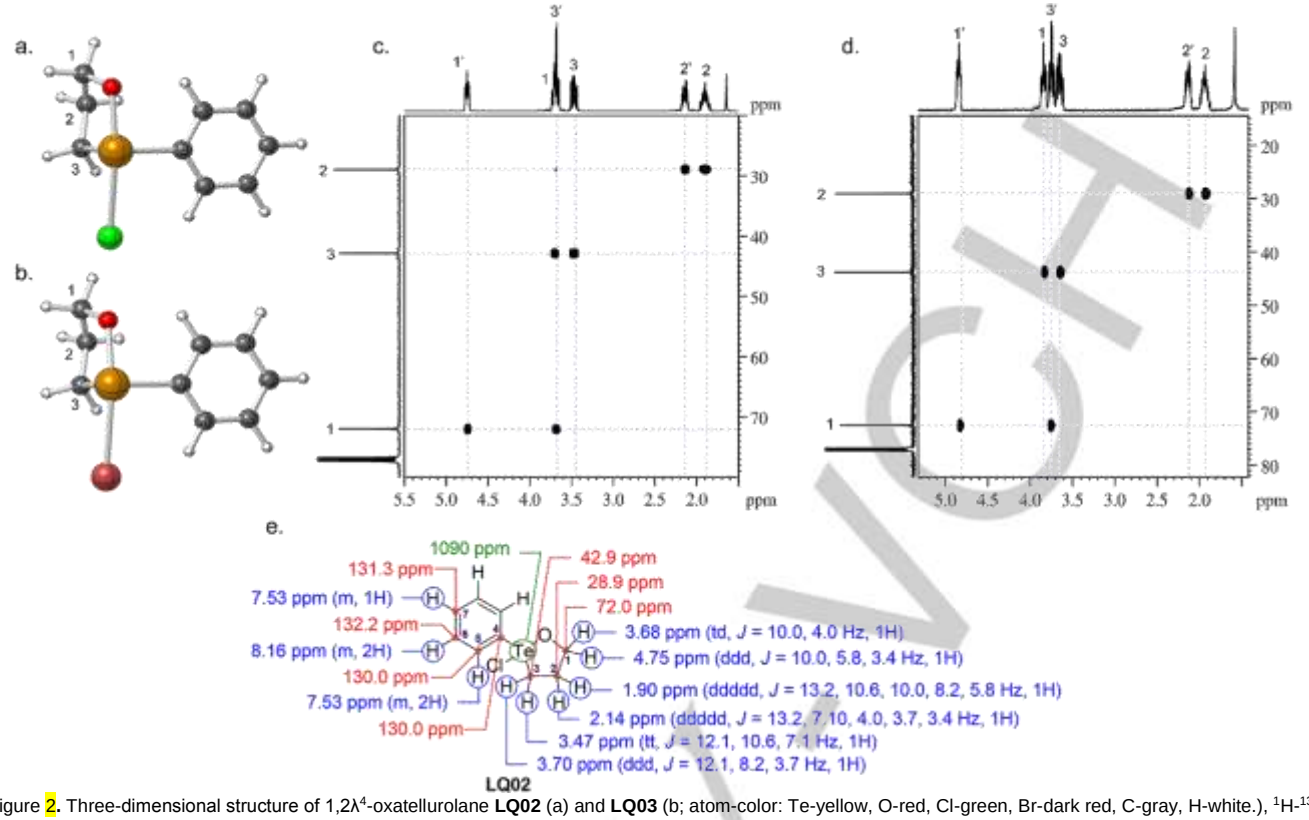

Figure 2. Three-dimensional structure of 1,2λ⁴-oxatellurolane **LQ02** (a) and **LQ03** (b; atom-color: Te-yellow, O-red, Cl-green, Br-dark red, C-gray, H-white.), ^{1}H-^{13}C HSQC correlation maps for **LQ02** (c) and **LQ03** (d) and chemical shift on ^{1}H (blue), ^{13}C (red) and ^{125}Te (green) NMR analyses for **LQ02** (e).

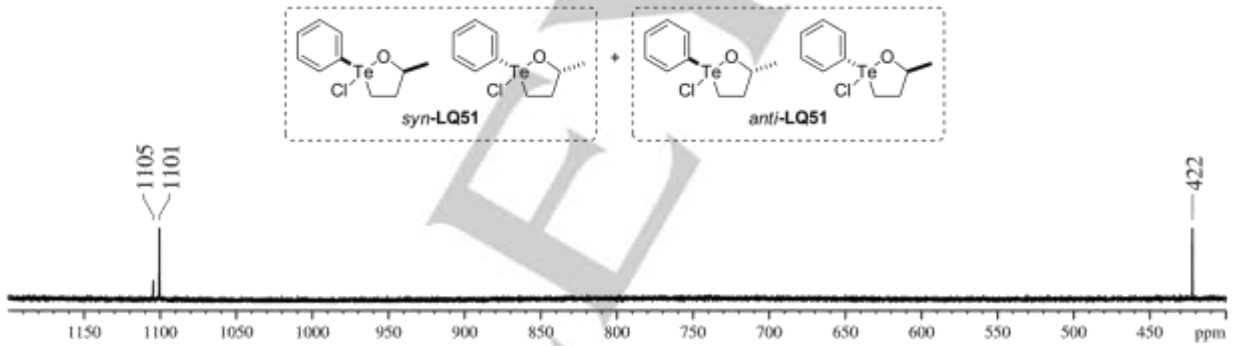

Figure 3. ^{125}Te NMR spectrum (126.24 MHz, $CDCl_3$, PhTeTePh (δ = 422)) of 1,2λ⁴-oxatellurolane **LQ51**.

3 and 4) changed from 5.1 and 109.4 ppm to 43.2 and 128.1 ppm, respectively, after oxidation of hydroxy telluride **3a** to **LQ02** (See Supporting Information). The most significant difference of chemical shift after the oxidation step was observed in ^{125}Te NMR analyses, in which the chemical shift varied from 473 ppm (**3a**) to 1090 ppm (**LQ02**).

Formation of diastereoisomers for two-chirality center-containing compounds was confirmed by the presence of two signals in ^{125}Te NMR spectra, as exemplified by **LQ51** spectrum in Figure 3. The difference in intensity between those signals demonstrated some degree of diatereoselectivity during the cyclization step. Signals at δ = 1101 and δ = 1105 are in accordance with chemical shifts obtained for the other synthesized tellurium(IV)-containing heterocycles and indicate that one of diastereoisomers (*syn*-**LQ51** or *anti*-**LQ51)** was preferentially formed.

Single-crystal X-ray Crystallography

Single-crystal X-ray diffraction analysis for representative compounds confirmed the cyclization products (Figure 4). Both **LQ02** (Figure 4a) and **LQ51** (Figure 4c) presented two independent molecules, which are enantiomers, in their crystals, and **LQ49** (Figure 4b) and **LQ56** (Figure 4d) are in centrosymmetric space groups and these crystals therefore contain both enantiomers too. Selected bons and crystallographic data are listed in Tables 1 and 2. The structures revealed that all the compounds adopted a seesaw-molecular geometry about the Te atom, typical for the hypervalent center of Te(IV).[19c, 20] Hypervalent O–Te–Cl bonding presented average 2.00 and 2.66 Å lengths for Te–O (Te1–O1 and Te2–O2, entries 1 and 2, Table 1) and Te–Cl (Te1–Cl1 and Te2–Cl2, entries 3 and 4) with an average 170° angle (O1–Te1– Cl1 and O2–Te2–Cl2, entries 9 and 10). Te–C bonds at the equatorial positions had an average 2.13 Å length (entries 5-8) and an average 96° angle for C–Te–C (entries 11 and 12). The chelating angles, between axial and equatorial positions of type O–Te–C (O1–Te1–C10 and O2–Te2–C20, entries 13 and 14, Table 1) presented an average of 98° angle.

10.1002/chem.202102287

RESEARCH ARTICLE

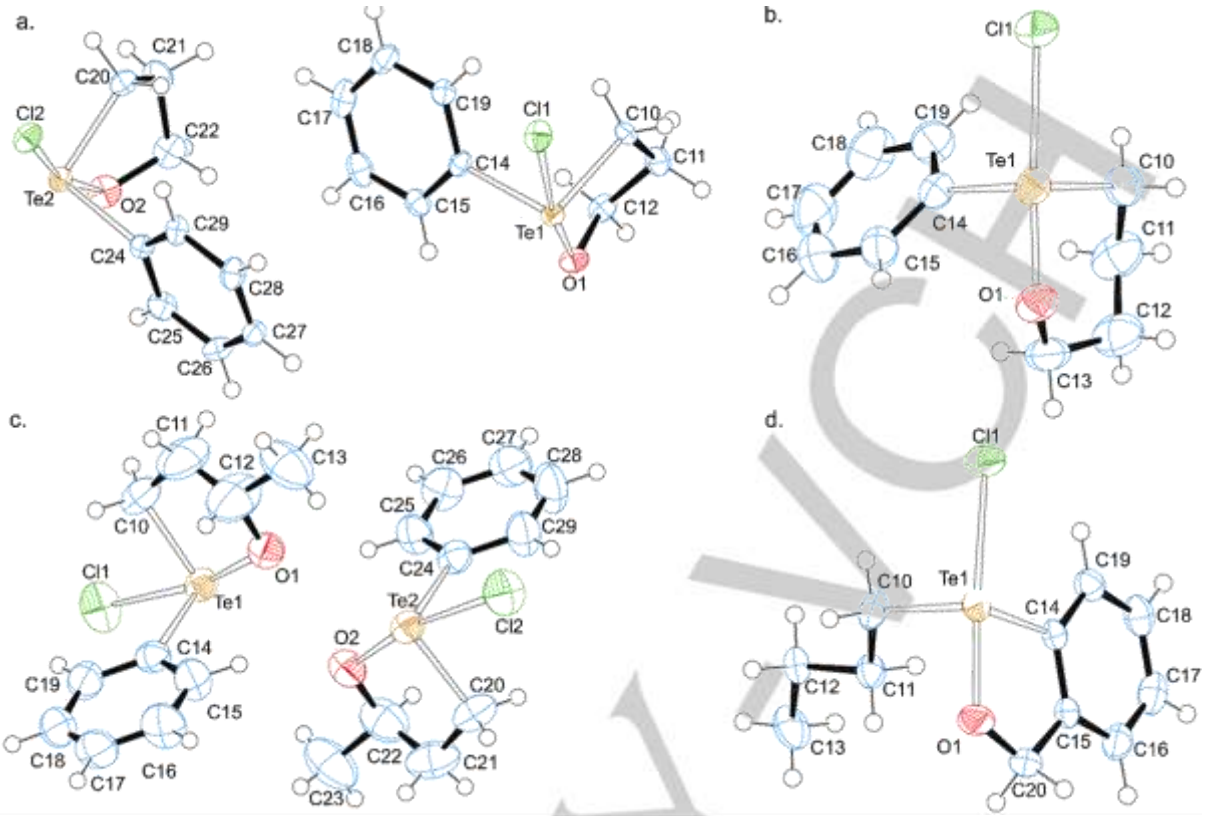

Figure 4. ORTEP[21] representation of **LQ02** (a), **LQ49** (b), **LQ51** (c) and **LQ56** (d). Thermal ellipsoids are drawn at the 50% probability level. Atom-color: Te-yellow, O-red, Cl-green, C- blue, H-white.

Table 1. Selected Bond Lengths (Å) and Angles (°) for organotelluranes **LQ02**, **LQ49**, **LQ51,** and **LQ56**.

Entry	Compound	LQ02[a]	LQ49	LQ51[a]	LQ56
		Bond Lengths Lengths (Å)			
1	Te1–O1	2.011(4)	1.983(2)	1.995(4)	2.009(3)
2	Te2–O2	2.000(5)	-	1.993(4)	-
3	Te1–Cl1	2.642(2)	2.6752(9)	2.653(2)	2.6353(11)
4	Te2–Cl2	2.6811(14)	-	2.664(2)	-
5	Te1–C10	2.136(5)	2.134(3)	2.129(5)	2.140(4)
6	Te2–C20	2.144(7)	-	2.118(5)	-
7	Te1–C14	2.132(7)	2.126(3)	2.134(5)	2.111(4)
8	Te2–C24	2.130(7)	-	2.120(6)	-
		Angles (°)			
9	O1–Te1–Cl1	170.16(14)	175.68(8)	168.55(11)	170.70(10)
10	O2–Te2–Cl2	165.5(2)	-	169.02(11)	-
11	C10–Te1–C14	94.8(3)	96.12(13)	96.2(2)	98.2(2)
12	C20–Te2–C24	95.5(3)	-	95.6(2)	-
13	O1–Te1–C10	84.5(2)	91.91(13)	83.6(2)	91.5(2)
14	O2–Te2–C20	83.5(2)	-	84.2(2)	-

[a] There are two independent molecules (enantiomers) in the crystal.

Table 2. Crystal and structure refinement data for organotellurane **LQ02**, **LQ49**, **LQ51,** and **LQ56**.

	LQ02	**LQ49**	**LQ51**	**LQ56**
Empirical formula	$C_9H_{11}ClOTe$	$C_{10}H_{13}ClOTe$	$C_{10}H_{13}ClOTe$	$C_{11}H_{15}ClOTe$
Molecular weight (g mol^{-1})	298.23	312.25	312.25	326.28
Temperature (K)	173(2)	301(2)	302(2)	200(2)
Crystal system	Orthorhombic	Orthorhombic	Orthorhombic	Monoclinic
Space group	$Pca2_1$	Pbca	$Pna2_1$	$P2_1/c$
a (Å)	8.6680(4)	10.4460(4)	13.3710(6)	8.4594(6)
b (Å)	9.7474(5)	9.0554(4)	16.9537(9)	16.8778(12)
c (Å)	23.1440(11)	23.4543(11)	10.0889(6)	8.7897(6)
β (°)	90	90	90	108.582(2)
V (Å^3)	1955.45(16)	2218.61(17)	2287.0(2)	1189.54(15)
Z	8	8	8	4
μ (mm^{-1})	26.126	2.882	2.796	21.535
θ_{max}	74.979	27.498	27.500	74.957
Reflections collected	136558	170329	150955	70700
Independent reflections	4020	2543	5227	2447
R_{int}	0.084	0.051	0.046	0.076
Reflections with $I > 2\sigma_I$	3909	2245	4742	2387
R_1 ($I > 2\sigma_I$)*	0.026	0.027	0.021	0.033
wR_2 ($I > 2\sigma_I$)*	0.066	0.063	0.048	0.093
R_1 all data[a]	0.026	0.033	0.027	0.034
wR_2 all data[a]	0.067	0.065	0.050	0.093
Goodness-of-fit on F^2	1.057	1.154	1.066	1.087
Largest diff. peak and hole (e Å^{-3})	1.28, -0.60	0.92, -0.81	0.52, -0.40	2.05, -0.81

[a] As defined by the SHELXL program.[22]

Mechanistic Studies

To further investigate the oxidation-cyclization step for the tellurium-containing heterocycles formation (Scheme 1, step iii), a mechanistic study employing DFT calculations was performed for **LQ02** (see Experimental Section in Supporting Information for computational details). First, the transition state structure (TSS) involved in the oxidation step (**TSS1**) was located, consistent with the chlorine atom transfer from NCS to the Te atom of hydroxy telluride **3a** forming a new Te–Cl bond with a low energy barrier (4.9 kcal mol^{-1}), as shown in Figure 5.

Intrinsic reaction coordinate (IRC) calculations indicated that the Te–Cl bond is 69% formed at the **TSS1** as observed in Figure 6. Moreover, results suggest significant changing of the Cl–Te···O angle along this step — ranging from 137° at the reactants to 165° when intermediate is formed (Figure 6) — which was attributed to the formation of strong Te···O interaction. Natural Bond Orbitals (NBO) calculations confirmed this hypothesis, revealing electron density donation from oxygen atom to tellurium atom resulting in a 28.7 kcal mol^{-1} n(O) → σ*(Te–Cl) interaction, indicating a chalcogen bonding of 2.39 Å[23]. Results also suggest a highly structural resemblance between protonated intermediate (**I**) and the final product **LQ02**. In fact, the O–H bond is responsible for preventing the formation of **LQ02**, as revealed by comparing Te···O and Te–Cl distances and bond lengths: Te–Cl bond increases 0.26 Å from **I** to **LQ02**, whereas the Te···O distance was shortened by 0.37 Å after deprotonation, which suggests the formation of a new O–Te–Cl hypervalent bond.

Then we turned our attention to the cyclization step. After several attempts, TSS (**TSS2**) was located. IRC calculations suggest a complex intermediate (**I'**) in the reverse direction, formed by coordination of oxygen atom of succinimide ion (NS^-) to tellurium atom of **I** (Figure 5 and 6). Since complex **I** is not conformationally appropriate for the formation of **I'**, it is likely that that another NS^- anion could be involved in the formation of the latter (coming from reaction occurring nearby), not necessarily the leaving group formed in the oxidation step. After the release of NS^-, the

10.1002/chem.202102287

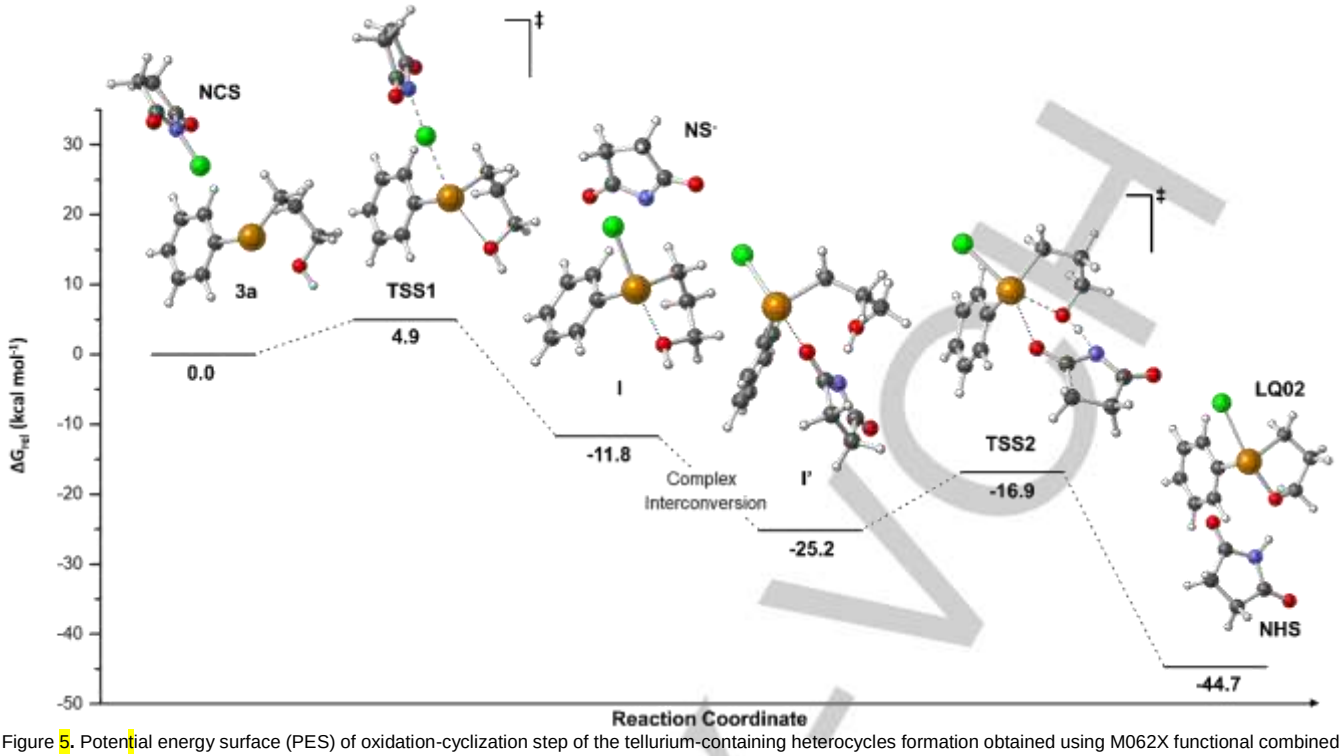

Figure 5. Potential energy surface (PES) of oxidation-cyclization step of the tellurium-containing heterocycles formation obtained using M062X functional combined with LANL2DZ (for Te atom) and 6-311++G(d,p) (for additional atoms). Atom-color: Te-yellow, O-red, Cl-green, N-blue, C-gray, H-white.

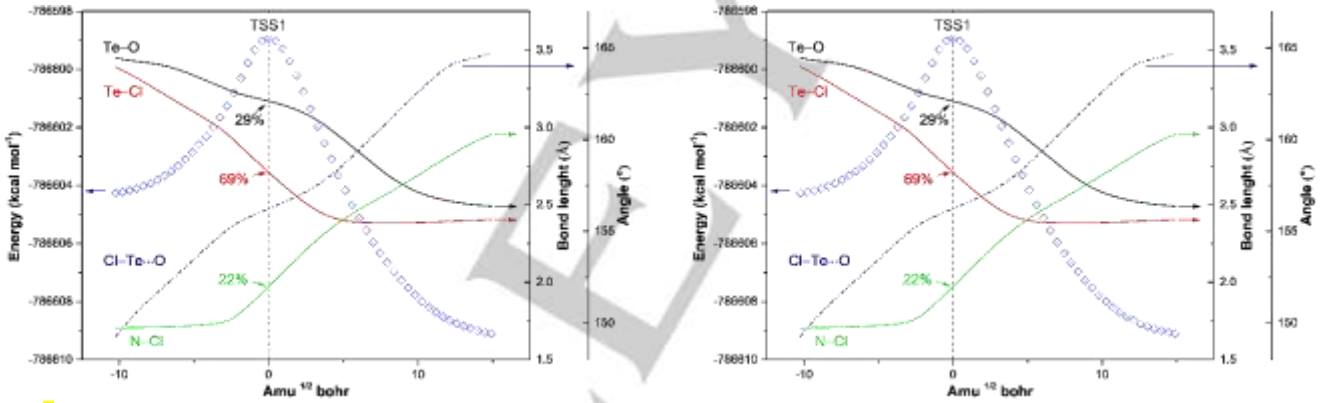

Figure 6. Optimized **TSS1** and **TSS2** IRC plot obtained with M062X combined with LANL2DZ (Te) and 6-311++G(d,p) basis sets.

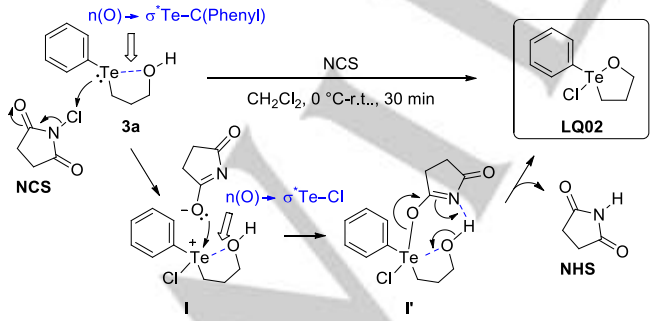

Figure 7. Proposed mechanism for the formation of **LQ02**.

formation of **I'** is likely to occur in a barrierless process, since a chalcogen interaction (HO···Te) in **I** is replaced by a Te–O covalent bond and an OH···N hydrogen bonding or, in other words, a very energetically favorable formation of **I'** should be expected. Moreover, complex I features a positive tellurium center, which makes it a great electrophile. Energy barrier of 8.3 kcal mol^{-1} to reach **TSS2** from **I'** was observed. Calculations revealed a concerted cyclization step involving the formation of the Te–O bond in **LQ02** and the proton transfer from hydroxyl group to the nitrogen atom of NS$^-$, with elimination of succinimide (NHS). The complete mechanistic proposal is presented in Figure 7. IRC plot presented in Figure 6 indicates that 48% of the Te–O bond was formed at the **TSS2** whereas 25% of the Te–O···NS$^-$ interaction was broken, consistent with a highly asynchronous pathway. This is also supported by the proton transfer of the O–H group to the NS$^-$ anion, which is only 2% completed at the **TSS2**. Uniform Te–Cl bond elongation along reaction pathway was also observed. The formation of the N–H bond is the last critical event of the cyclization process, finally releasing the products. The oxidation process was found as the rate-determining step and the low barrier of 4.9 kcal mol^{-1} is consistent with the reaction occurring at 0 °C.

Explaining the diastereoselectivity in LQ51 formation

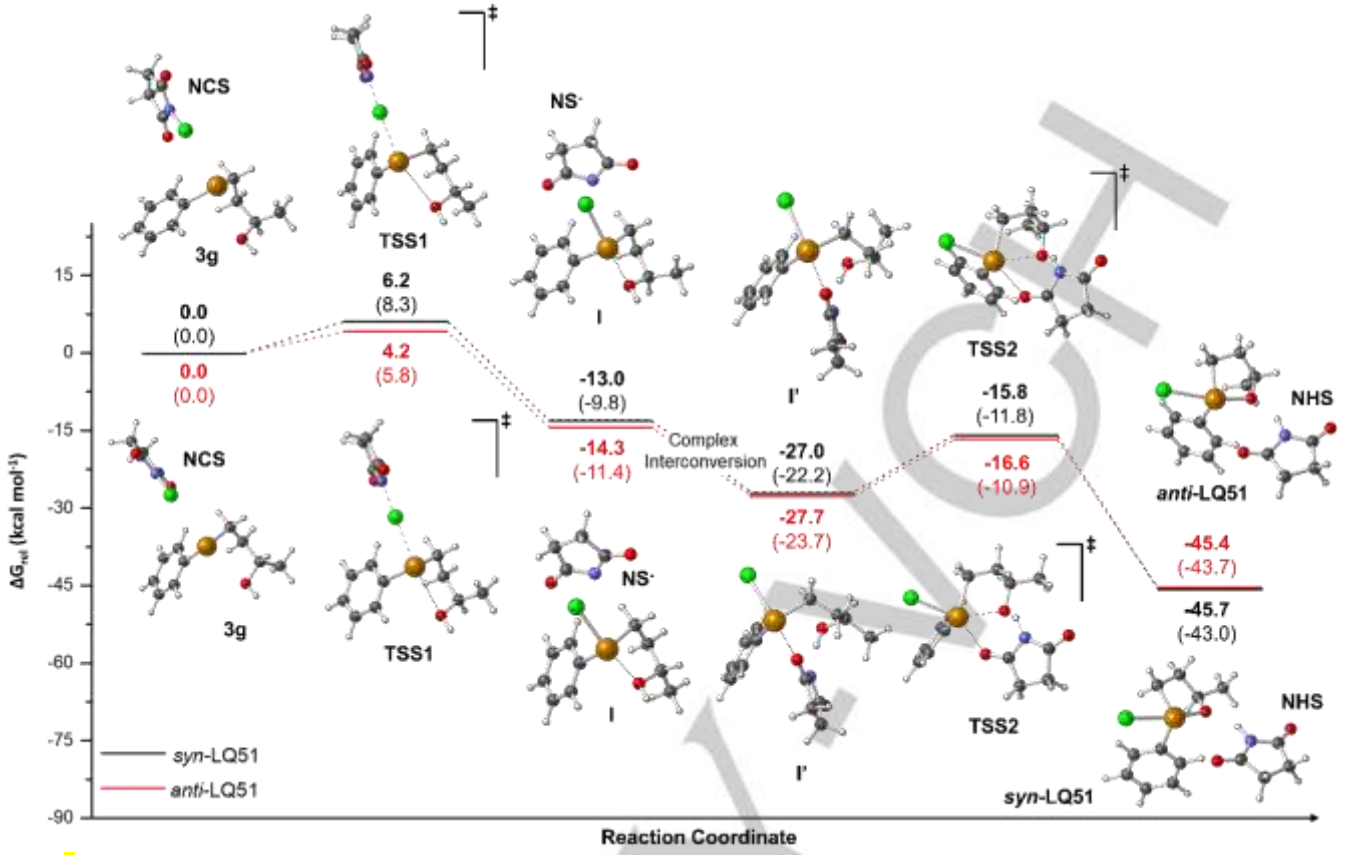

Figure 8. PES of oxidation-cyclization step of the *anti*-**LQ51** and *syn*-**LQ51** formation obtained using M062X and single points using ωB97X-D (in parentheses) functional combined with LANL2DZ (for Te atom) and 6-311++G(d,p) (for additional atoms). Atom-color: Te-yellow, O-red, Cl-green, N-blue, C-gray, H-white.

1,2λ^4-oxatellurolane **LQ51** is a two-chirality center-containing compound, so a pair of diastereoisomers is also expected in its preparation. Indeed, the two signals were observed in ^{125}Te NMR spectra of **LQ51** at 1101 and 1105 ppm (Figure 3) indicating a highly degree of diastereoselectivity. A 1:4 ratio between diastereoisomers was determined using the relative areas of some equivalent signs at 2.34 and 2.39, 3.50 and 3.61 and 8.16 and 8.21 ppm in the ^{1}H NMR spectrum (600.13 MHz, $CDCl_3$, TMS) (see on Figures S88-91 in Supporting Information). Supported by this experimentally observed selectivity and the failure to assign NMR signals to diastereoisomer groups, a mechanistic study employing DFT calculations were also carried out to rationalize the diastereoselectivity and identify the diastereoisomers preferably formed (*syn*-**LQ51** or *anti*-**LQ51**, Figure 3).

TSSs for the oxidation (**TSS1**) and the cyclization steps (**TSS2**) were located for each diastereoisomer (*syn*-**LQ51** or *anti*-**LQ51**) as shown in Figure 8. Similar Potential energy surface (PES) and TSSs were obtained for both diastereoisomers of **LQ51** compared to **LQ02** (vide supra). For the oxidation step involved in the formation of *anti*-**LQ51**, calculations revealed an energy barrier of 4.2 kcal mol^{-1}, which is 2.0 kcal mol^{-1} lower that that observed for the diastereoisomer *syn*-**LQ51** (Figure 8). Such significant difference in the rate determinant step of the reactions corroborates the preferential formation of one of the diastereoisomers, as indicated by NMR analyses. Single point energy calculations using ωB97X-D[24] were also performed for the stationary points involved in the rate determinant step and similar results were observed. Thus, based on theoretical calculations, *anti*-**LQ51** corresponds to the major diastereoisomer formed and observed experimentally in the ^{125}Te NMR spectra at 1101 ppm, while the *syn*-**LQ51** is the minor diastereoisomer with signal at 1105 ppm.

Antiprotozoal Activity of Tellurium (IV)-containing Heterocycles

Hypervalent Te-containing **LQ02-04**, **LQ33-35,** and **LQ48-57** were submitted to *in vitro* assays against *Leishmania amazonensis* promastigotes, and miltefosine was used as the positive control (Table 3). Antileishmanial activities were expressed as IC_{50} values - the inhibitory concentration able to cause the death of 50% of the parasites in relation to the negative control (non-treated infected cells) - and the cytotoxic of the compounds were expressed as CC_{50} - the concentration able to kill 50% of the cells (J774A1 macrophages) in relation to the untreated cell control. The selectivity indexes (SI) were determined as the ratio between the CC_{50} in macrophages and the corresponding IC_{50} value in promastigotes, allowing to determine how many times the assayed compound was more selective against the protozoa than to the mammalian host cell(macrophages).

1,4-Substituted 1,2λ^4-oxatellurolanes showed higher activity and selective (expressed by SI) in comparison to unsubstituted analogs **LQ02** (SI: 1, entry 1, Table 2) and **LQ03** (inactive; entry 2, Table 2). In particular, R' = OMe (**LQ04**, SI: 7, entry 3, Table 2**)** and R' = Cl (**LQ33** and **LQ34**, SI: 5, entries 4 and 5, Table 2) presented higher SI than miltefosine (SI: 3, entry 17, Table 2). **LQ35** (R' = F) exhibited the same value of SI as miltefosine (Figure 9). **LQ48** and **LQ51-55** were considered non-promising compounds due to low SI values observed ($\leq$ 2; entries 7-12, Table 2).

Table 3. *In vitro* Activity toward *L. amazonensis* promastigotes, Cytotoxicity in macrophages, and Selectivity Indexes of **LQ02-04**, **LQ33-35** and **LQ48-57**.[a]

Entry	Subst.	X	R	R'	IC_{50} ± SD (µmol L^{-1})[b]	CC_{50} ± SD (µmol L^{-1})[c]	SI[d]
				1,2λ⁴-oxatellurolanes: 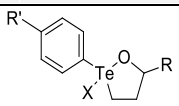			
1	**LQ02**	Cl	H	H	34.7 ± 10.6	23.1 ± 2.8	1
2	**LQ03**	Br	H	H	>100[e]	7.8 ± 2.1	-[f]
3	**LQ04**	Cl	H	OMe	7.0 ± 1.3	51.3 ± 12.4	7
4	**LQ33**	Cl	H	Cl	13.0 ± 4.2	64.0 ± 8.3	5
5	**LQ34**	Br	H	Cl	9.7 ± 0.3	43.7 ± 2.5	5
6	**LQ35**	Cl	H	F	7.7 ± 2.3	23.3 ± 2.5	3
7	**LQ48**	Cl	H	Ketal[g]	31.4 ± 7.4	20.7 ± 7.4	1
8	**LQ51**	Cl	Me	H	35.0 ± 3.1	34.0 ± 4.9	1
9	**LQ52**	Br	Me	H	>100[e]	19.1 ± 2.1	-[f]
10	**LQ53**	Cl	Ph	H	6.3 ± 0.3	13.9 ± 2.5	2
11	**LQ54**	Cl	H	Ac	32.8 ± 6.4	13.7 ± 3.7	0.4
12	**LQ55**	Cl	H	Oxime[h]	41.5 ± 7.0	58.0 ± 14.2	1
				1,2λ⁴-oxatelluranes: 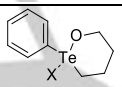			
13	**LQ49**	Cl	-	-	8.6 ± 2.5	31.0 ± 7.8	4
14	**LQ50**	Br	-	-	4.1 ± 1.0	49.0 ± 5.0	12
				1,2λ⁴-benzoxatelluroles: 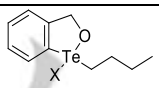			
15	**LQ56**	Cl	-	-	5.7 ± 0.3	32.0 ± 6.2	6
16	**LQ57**	Br	-	-	>100[e]	16.0 ± 2.5	-[f]
17	Miltefosine	-	-		20.7 ± 0.2	55.0 ± 1.9	3

[a] Data were expressed as the mean ± SD determined from three independent experiments. [b] IC_{50}: the concentration that inhibit 50% of parasite growth in relation to the untreated control. [c] CC_{50}: cytotoxic concentration able to kill 50% of the macrophages in relation to the untreated control. [d] Selectivity index: CC_{50}/IC_{50}. [e] Considered inactive. [f] Not applicable. [g] 2-Methyl-1,3-dioxolan-2-yl group. [h] (*E*)-1-(hydroxyimino)ethyl group.

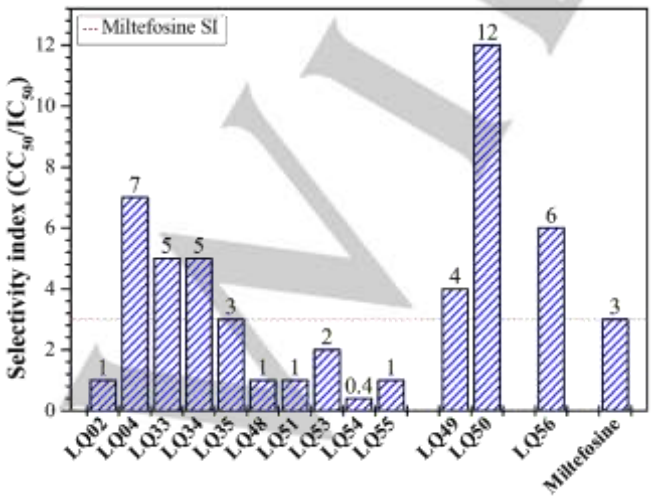

Figure 9. Selectivity indexes of assayed organotelluranes and miltefosine.

The unique two 1,2λ⁴-oxatelluranes assayed here, **LQ49** and **LQ50,** exhibited higher SI than miltefosine (Figure 9). The SI for **LQ49** was 4 (entry 13, Table 2), while **LQ50** was identified as the most selective substance in our series with SI = 12 (entry 14, Table 2). Among 1,2λ⁴-benzoxatelluroles, only the chlorinated **LQ56** was active (SI: 6, entry 15, Table 2) while its brominated congener **LQ57** was considered inactive, following the trend observed for 1,2λ⁴-oxatellurolanes **LQ02** and **LQ03**. **LQ50** presented the highest SI in the antileishmanial assays (SI = 12, entry 14, Table 2) and evidenced the great potential for Te-containing six-membered heterocycles. The best results observed for 1,2λ⁴-oxatellurolanes and 1,2λ⁴-benzoxatellurole were highlights in **LQ04** and **LQ56**, respectively. Besides, chlorinated 1,2λ⁴-oxatellurolanes and 1,2λ⁴-benzoxatellurole showed better performance than equivalent brominated Te-containing heterocycles, except for 1,2λ⁴-oxatelluranes **LQ49** and **LQ50**. Despite the absence of a clear pattern for structure-activity

10.1002/chem.202102287

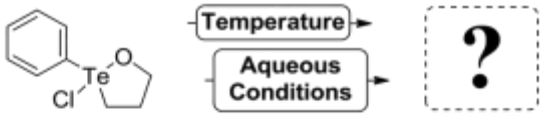

LQ02

Entry	Conditions	Temp. (°C)	δ ^{125}Te
1	DMSO-d_6[a]	25	1154
2	DMSO-d_6[a]	35	1148
3	DMSO-d_6[a]	45	1143
4	DMSO-d_6[a]	55	1137
5	DMSO-d_6[a]	65	1142
6	DMSO-d_6/H_2O[b]	25	1157

[a] 15 mg of **LQ02** in 500 µL of DMSO-d_6. [b] 40 mg of LQ02 in 500 µL of DMSO-d_6 and 100 µL H_2O (distilled water).

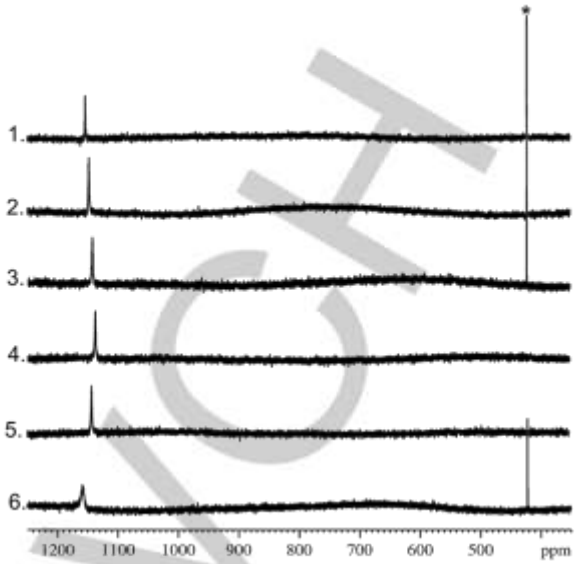

Figure 10. ^{125}Te NMR (126.24 MHz, DMSO-d_6, PhTeTePh (*, δ = 422)) on the stability assays for **LQ02.**

relationships, the three classes of hypervalent Te-containing heterocycles studied in this work - 1,2λ^4-oxatellurolanes (**LQ04**), 1,2λ^4-oxatelluranes (**LQ50**) and 1,2λ^4-benzoxatellurole **(LQ56)** - showed potential as antileishmanial agents.

Investigation of Hypervalent Tellurium-containing Heterocycles Stability.

In the literature, there is a debate about the stability of hypervalent tellurium compounds in organic-aqueous media.[9h, 25] So, complement stability assays for some representative compounds were also performed using ^{125}Te NMR as analytical tool. Initially, the thermal stability of **LQ02** in dimethyl sulfoxide-d_6 (DMSO-d_6) was investigated at temperatures ranging from 25 to 65 °C.[9h, 25a] The results obtained by ^{125}Te NMR are described in Figure 10, in which no significant changes in chemical shifts were observed, demonstrating the thermal stability of the studied organotellurane. Additionally, ^{1}H NMR analysis confirmed that the structure of **LQ02** remained intact. The same methodology was applied for **LQ51** to evaluate the possible cycle opening through variations between the proportion of diastereoisomers. However, satisfactorily no structural change was observed even after 5 hours in reflux in $CDCl_3$ (see on Supporting Information, figure S110).

In the sequence, **LQ02** was solubilized in DMSO-d_6, followed by distilled water addition (Figure 10).^{125}Te NMR analyses presented a single signal at δ = 1157, again suggesting no chemical structure variation. Recovery and ^{1}H NMR analysis of **LQ02** confirmed no structural modifications in organic-aqueous media. Since the tested organotelluranes did not suffer opening cycle and parallel undesired reactions up to 65 °C, including in organic-aqueous media, as observed for other telluranes,[24a, b, d] in association with the promising results of biological activity, 1,2λ^4-oxatellurolane, 1,2λ^4-benzoxatellurole and especially 1,2λ^4-oxatellurane studied in this work present great potential in the search for biologically active Te-containing compounds.

Conclusion

In summary, eleven chlorinated and five brominated compounds – thirteen unpublished – hypervalent Te-containing heterocycles (**LQ02-04**, **LQ33-35,** and **LQ48-57)** have been successfully synthesized in 0.4% to 40% overall yields and **LQ02**, **LQ49**, **LQ51,** and **LQ56** structures were elucidated by NMR analysis and single-crystal X-ray diffraction methods. Computational results revealed that the oxidation-cyclization proceeds via two-step mechanism: (1) the oxidation of the hydroxy telluride by NCS as the rate determinant step with energy barrier of 4.9 kcal mol^{-1} and (2) cyclization involving the formation of the new Te–O bond and the O–H bond break in a concerted asynchronous fashion. Additionally, the diastereoselectivity observed was rationalized using theoretical calculations, allowing the identification of *anti*-**LQ51** as the major diastereoisomer formed.

In vitro activity assays against *L. amazonensis* promastigotes showed that 1,2λ^4-oxatellurane **LQ50** (SI = 12), 1,2λ^4-oxatellurolane **LQ04** (SI = 7) and 1,2λ^4-benzoxatellurole **LQ56** (SI = 6) were the most promising substances, with SI values higher than that observed for miltefosine. Six-membered 1,2λ^4-oxatellurane presented better results than five-membered Te-containing heterocycles (1,2λ^4-oxatellurolane and 1,2λ^4-benzoxatellurole), suggesting this as a more promising class for future investigations. ^{125}Te and ^{1}H NMR analysis showed **LQ02** and **LQ51** as thermal stable (up to 65 °C) and in aqueous-organic conditions. In conclusion, this work aims to contribute to the search for bioactive organotellurium compounds and highlight the biological potential of the hypervalent Te-containing heterocycles.

Acknowledgements

The authors thank the National Council for Scientific and Technological Development (CNPq, Brazil), and the Coordination for the Improvement of Higher Level Personnel (CAPES, Brazil) for financial support and fellowships of J. P. A. Souza, P. T. Bandeira, L. R. A. Menezes, M. B. Bespalhok, D. B. Scariot, F.P. Garcia, D. L. Hughes and S. O. K. Giese.

Keywords: Hypervalent Tellurium compounds • Oxidation-

Cyclization Mechanism • Leishmanicidal activity • ^{125}Te NMR

[1] L. A. Ba, M. Döring, V. Jamier, C. Jacob, *Org. Biomol. Chem.* **2010**, *8*, 4203–4216.

[2] a) S. E. Ramadan, A. A. Razak, A. M. Ragab, M. El-Meleigy, *Biol. Trace Elem. Res.* **1989**, *20*, 225–232; b) J. O. Boles, L. Lebioda, R. B. Dunlap, J. D. Odom, *SAAS Bull. Biochem. Biotechnol.* **1995**, *8*, 29–34; c) N. Budisa, B. Steipe, P. Demange, C. Eckerskorn, J. Kellermann, R. Huber, *Eur. J. Biochem.* **1995**, *230*, 788–796.

[3] a) L. J. Edgar, R. N. Vellanki, A. Halupa, D. Hedley, B. G. Wouters, M. Nitz, *Angew. Chem. Int. Ed.* **2014**, 53, 11473 –11477. b) L. M. Lee, M. Tsemperouli, A. I. Poblador-Bahamonde, S. Benz, N. Sakai, K. Sugihara, S. Matile, *J. Am. Chem. Soc*. **2019**, 141, 810−814.

[4] a) C.-M. Andersson, A. Hallberg, R. Brattsand, I. A. Cotgreave, L. Engman, J. Persson, *Bioorg. Med. Chem. Lett.* **1993**, *3*, 2553–2558; b) C.-M. Andersson, R. Brattsand, A. Hallberg, L. Engman, J. Persson, P. Moldéus, I. Cotgreave, *Free Radic. Res.* **1994**, *20*, 401–410; c) R. L. O. R. Cunha, I. E. Gouvea, L. Juliano, *An. Acad. Bras. Cienc.* **2009**, *81*, 393–407; d) T. G. Back, D. Kuzma, M. Parvez, *J. Org. Chem.* **2005**, *70*, 9230–9236; e) E. E. Alberto, V. Do Nascimento, A. L. Braga, *J. Braz. Chem. Soc.* **2010**, *21*, 2032–2041; f) M. Doering, L. A. Ba, N. Lilienthal, C. Nicco, C. Scherer, M. Abbas, A. A. P. Zada, R. Coriat, T. Burkholz, L. Wessjohann, M. Diederich, F. Batteux, M. Herling, C. Jacob, *J. Med. Chem.* **2010**, *53*, 6954–6963; g) S. Kumar, H. Johansson, T. Kanda, L. Engman, T. Müller, H. Bergenudd, M. Jonsson, G. F. Pedulli, R. Amorati, L. Valgimigli, *J. Org. Chem.* **2010**, *75*, 716–725; h) R. Amorati, G. F. Pedulli, L. Valgimigli, H. Johansson, L. Engman, *Org. Lett.* **2010**, *12*, 2326–2329; i) P. T. Bandeira, M. C. Dalmolin, M. M. de Oliveira, K. C. Nunes, F. P. Garcia, C. V. Nakamura, A. R. M. de Oliveira, L. Piovan, *Bioorg. Med. Chem.* **2019**, *27*, 410–415.

[5] a) B. Sredni, R. R. Caspi, A. Klein, Y. Kalechman, Y. Danziger, M. BenYa'akov, T. Tamari, F. Shalit, M. Albeck, *Nature* **1987**, *330*, 173–176; b) B. Sredni, R.-H. Xu, M. Albeck, U. Gafter, R. Gal, A. Shani, T. Tichler, J. Shapira, I. Bruderman, R. Catane, B. Kaufman, J. K. Whisnant, K. L. Mettinger, Y. Kalechman, *Int. J. Cancer* **1996**, *65*, 97–103.

[6] a) M. Daniel-Hoffmann, M. Albeck, B. Sredni, Y. Nitzan, *Arch. Microbiol.* **2009**, *191*, 631–638; b) I. E. Gouvea, J. A. N. Santos, F. M. Burlandy, I. L. S. Tersariol, E. E. da Silva, M. A. Juliano, L. Juliano, R. L. O. R. Cunha, *Biol. Chem.* **2011**, *392*, 587–591; c) M. Daniel-Hoffmann, B. Sredni, Y. Nitzan, *J. Antimicrob. Chemother.* **2012**, *67*, 2165–2172; d) F. M. Libero, M. C. D. Xavier, F. N. Victoria, P. S. Nascente, L. Savegnago, G. Perin, D. Alves, *Tetrahedron Lett.* **2012**, *53*, 3091–3094; e) R. Yalew, D. Kenigsbuch-Sredni, B. Sredni, Y. Nitzan, *Arch. Microbiol.* **2014**, *196*, 51–61; f) W. A. Al-Masoudi, R. H. Al-Asadi, R. M. Othman, N. A. Al-Masoudi, *Eur. J. Chem.* **2015**, *6*, 374–380; g) S. El Chamy Maluf, P. M. S. Melo, F. P. Varotti, M. L. Gazarini, R. L. O. R. Cunha, A. K. Carmona, *Parasitol. Int.* **2016**, *65*, 20–22; h) Â. Sena-Lopes, R. N. das Neves, F. S. B. Bezerra, M. T. de Oliveira Silva, P. C. Nobre, G. Perin, D. Alves, L. Savegnago, K. R. Begnini, F. K. Seixas, T. Collares, S. Borsuk, *Biomed. Pharmacother.* **2017**, *89*, 284–287; i) L. F. Reis de Sá, F. T. Toledo, A. C. Gonçalves, B. A. Sousa, A. A. dos Santos, P. F. Brasil, V. A. Duarte da Silva, A. C. Tessis, J. A. Ramos, M. A. Carvalho, E. Lamping, A. Ferreira-Pereira, *Antimicrob. Agents Chemother.* **2017**, *61*, 1–14; j) A. Malik, G. Goyat, K. K. Verma, S. Garg, *Chem. Sci. Trans.* **2018**, *7*, 329–337; k) F. Pinheiro, V. Bortolotto, S. Araujo, M. Poetini, C. Sehn, J. é Neto, G. Zeni, M. Prigol, *J. Microbiol. Biotechnol.* **2018**, *28*, 1209–1216.

[7] M. Brodsky, G. Halpert, M. Albeck, B. Sredni, *J. Inflamm.* **2010**, *7*, 3

[8] a) Y. Kalechman, D. L. Longo, R. Catane, A. Shani, M. Albeck, B. Sredni, *Int. J. Cancer* **2000**, *86*, 281–288; b) L. Engman, N. Al-Maharik, M. McNaughton, A. Birmingham, G. Powis, *Anticancer. Drugs* **2003**, *14*, 153–161; c) L. Engman, N. Al-Maharik, M. McNaughton, A. Birmingham, G. Powis, *Bioorg. Med. Chem.* **2003**, *11*, 5091–5100; d) B. Sredni, R. Gal, I. J. Cohen, J. Dazard, D. Givol, U. Gafter, B. Motro, S. Eliyahu, M. Albeck, H. M. Lander, Y. Kalechman, *FASEB J.* **2004**, *18*, 1–30; e) R. HAYUN, S. SHPUNGIN, H. MALOVANI, M. ALBECK, E. OKUN, U. NIR, B. SREDNI, *Ann. N. Y. Acad. Sci.* **2007**, *1095*, 240–250; f) H.-L. Seng, E. R. T. Tiekink, *Appl. Organomet. Chem.* **2012**, *26*, 655–662; g) P. Du, N. E. B. Saidu, J. Intemann, C. Jacob, M. Montenarh, *Biochim. Biophys. Acta - Gen. Subj.* **2014**, *1840*, 1808–1816; h) H. Danoch, Y. Kalechman, M. Albeck, D. L. Longo, B. Sredni, **2015**, 411–423; i) A. Silberman, Y. Kalechman, S. Hirsch, Z. Erlich, B. Sredni, A. Albeck, *ChemBioChem* **2016**, *17*, 918–927; j) T. Paschoalin, A. A. Martens, Á. T. Omori, F. V. Pereira, L. Juliano, L. R. Travassos, G. M. Machado-Santelli, R. L. O. R. Cunha, *Bioorg. Med. Chem.* **2019**, *27*, 2537–2545.

[9] a) A. Albeck, H. Weitman, B. Sredni, M. Albeck, *Inorg. Chem.* **1998**, *37*, 1704–1712; b) R. L. O. R. Cunha, M. E. Urano, J. R. Chagas, P. C. Almeida, C. Bincoletto, I. L. S. Tersariol, J. V. Comasseto, *Bioorg. Med. Chem. Lett.* **2005**, *15*, 755–760; c) R. L. O. R. Cunha, I. E. Gouvêa, G. P. V. Feitosa, M. F. M. Alves, D. Brömme, J. V. Comasseto, I. L. S. Tersariol, L. Juliano, *Biol. Chem.* **2009**, *390*, 1205–1212; d) L. Piovan, M. F. M. Alves, L. Juliano, D. Brömme, R. L. O. R. Cunha, L. H. Andrade, *J. Braz. Chem. Soc.* **2010**, *21*, 2108–2118; e) L. Piovan, M. F. M. Alves, L. Juliano, D. Brömme, R. L. O. R. Cunha, L. H. Andrade, *Bioorg. Med. Chem.* **2011**, *19*, 2009–2014; f) L. Piovan, L. Wu, Z.-Y. Zhang, L. H. Andrade, *Org. Biomol. Chem.* **2011**, *9*, 1347-1351; g) I. Caracelli, M. Vega-Teijido, J. Zukerman-Schpector, M. H. S. Cezari, J. G. S. Lopes, L. Juliano, P. S. Santos, J. V. Comasseto, R. L. O. R. Cunha, E. R. T. Tiekink, *J. Mol. Struct.* **2012**, *1013*, 11–18; h) L. Piovan, P. Milani, M. S. Silva, P. G. Moraes, M. Demasi, L. H. Andrade, *Eur. J. Med. Chem.* **2014**, *73*, 280–285.

[10] a) N. Furukawa, S. Sato, in *Chem. Hypervalent Compd.* (Ed.: Kiy-ya Akiba), New York, **1999**.; b) T. L. Brown, J. H. Eugene LeMay, B. E. Bursten, C. J. Murphy, P. M. Woodward, M. W. Stoltzfus, *Chemistry the Central Science*, New York, **2013**; c) T. Chivers, R. S. Laitinen, *Chem. Soc. Rev.* **2015**, *44*, 1725–1739.

[11] a) G. N. Lewis, *J. Am. Chem. Soc.* **1916**, *38*, 761–785; b) R. J. Gillespie, B. Silvi, *Coord. Chem. Rev.* **2002**, *233–234*, 53–62.

[12] a) R. J. Hach, R. E. Rundle, *J. Am. Chem. Soc.* **1951**, *73*, 4321–4324; b) G. C. Pimentel, *J. Chem. Phys.* **1951**, *19*, 446–448; c) J. I. Musher, *Angew. Chemie Int. Ed. English* **1969**, *8*, 54–68.

[13] M. M. L. Chen, R. Hoffmann, *J. Am. Chem. Soc.* **1976**, *98*, 1647–1653.

[14] a) B. Sredni, R. Geffen-Aricha, W. Duan, M. Albeck, F. Shalit, H. M. Lander, N. Kinor, O. Sagi, A. Albeck, S. Yosef, M. Brodsky, D. Sredni-Kenigsbuch, T. Sonino, D. L. Longo, M. P. Mattson, G. Yadid, *FASEB J.* **2007**, *21*, 1870–1883; b) E. Okun, T. V. Arumugam, S.-C. Tang, M. Gleichmann, M. Albeck, B. Sredni, M. P. Mattson, *J. Neurochem.* **2007**, *102*, 1232–1241; c) A. Carmely, D. Meirow, A. Peretz, M. Albeck, B. Bartoov, B. Sredni, *Hum. Reprod.* **2009**, *24*, 1322–1329; d) I. Sinuani, J. Weissgarten, I. Beberashvili, M. J. Rapoport, J. Sandbank, L. Feldman, M. Albeck, Z. Averbukh, B. Sredni, *Nephrol. Dial. Transplant.* **2009**, *24*, 2328–2338; e) D. Sheinboim, M. Hindiyeh, E. Mendelson, M. Albeck, B. Sredni, S. Dovrat, *Int. J. Mol. Med*. **2015**, *36*, 231–238; f) P. Vishwakarma, N. Parmar, P. Chandrakar, T. Sharma, M. Kathuria, P. K. Agnihotri, M. I. Siddiqi, K. Mitra, S. Kar, *Cell. Mol. Life Sci.* **2018**, *75*, 563–588.

[15] B. Turk, *Nat. Rev. Drug Discov.* **2006**, *5*, 785–799.

[16] A. Malik, G. Goyat, V. K. K. Verma, S. Garg, *Chem. Sci. Trans.* **2018**, 7, 329-337.

[17] C. B. C. Lima, W. W. Arrais-Silva, R. L. O. R. Cunha, S. Giorgio, *Korean J. Parasitol.* **2009**, *47*, 213.

[18] I. A. S. Pimentel, C. de S. Paladi, S. Katz, W. A. de S. Júdice, R. L. O. R. Cunha, C. L. Barbiéri, *PLoS One* **2012**, *7*, 1–7

[19] a) I. D. Sadekov, A. A. Maksimenko, A. V Zakharov, B. B. Rivkin, *Chem. Heterocycl. Compd.* **1994**, *30*, 243–253; b) I. D. Sadekov, A. A. Maksimenko, V. I. Minkin, *Tetrahedron* **1996**, *52*, 3365–3374; c) T. Takahashi, J. Zhang, N. Kurose, S. Takahashi, T. Koizumi, *Tetrahedron: Asymmetry* **1996**, *7*, 2797–2800; d) J. Zhang, S. Saito, T. Takahashi, T. Koizumi, *Heterocycles* **1997**, *45*, 575–584; e) J. Zhang, S. Saito, T. Koizumi, *J. Org. Chem.* **1998**, *63*, 5423–5429; f) S. Zhang, Y. Zhang, *Synth. Commun.* **2000**, *30*, 285–292.

[20] a) A. K. Singh, M. Kadarkaraisamy, G. . Murthy, J. Srinivas, B. Varghese, R. . Butcher, *J. Organomet. Chem.* **2000**, *605*, 39–44; b) J. Zukerman-Schpector, R. Cunha, Á. T. Omori, L. Sousa Madureira, E. R. T. Tiekink, *Acta Crystallogr. Sect. E Crystallogr. Commun.* **2017**, *73*, 564–568.

[21] a) Johnson, C. K.; ORTEP; Report ORNL-5138; Oak Ridge National Laboratory, Tennessee, USA, **1976**; b) L. J. Farrugia, *J. Appl. Crystallogr.* **2012**, *45*, 849–854.

[22] G. M. Sheldrick, *Acta Crystallogr. Sect. C Struct. Chem.* **2015**, *71*, 3–8.

10.1002/chem.202102287

[23] a) D. B. Werz, R. Gleiter, F. Rominger, *J. Am. Chem. Soc*. **2002**, *124*, 10638-10639; b) J. S. Murray, P. Lane, T. Clark, P. Politzer, *J. Mol. Model*. **2007**, *13*, 1033-1038; c) L. Vogel, P. Wonner, S. M. Huber, *Angew. Chem. Int. Ed*. **2019**, *7*, 1880-1891.

[24] A. Sengupta, K. Raghavachari, *Org. Lett.* **2017**, *19*, 2576–2579.

[25] a) M. S. Silva, L. H. Andrade, *Org. Biomol. Chem.* **2015**, *13*, 5924–5929; b) A. Silberman, M. Albeck, B. Sredni, A. Albeck, *Inorg. Chem.* **2016**, *55*, 10847–10850; c) C. R. Princival, M. V. L. R. Archilha, A. A. Dos Santos, M. P. Franco, A. A. C. Braga, A. F. Rodrigues-Oliveira, T. C. Correra, R. L. O. R. Cunha, J. V. Comasseto, *ACS Omega* **2017**, *2*, 4431–4439; d) M. L. Teixeira, L. R. A. Menezes, A. Barison, A. R. M. de Oliveira, L. Piovan, *J. Org. Chem.* **2018**, *83*, 7341–7346.

10.1002/chem.202102287

Entry for the Table of Contents

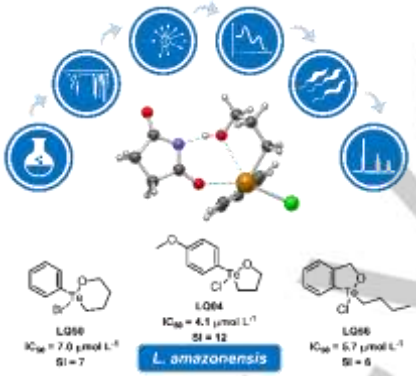

Promissory hypervalent Te(IV)-containing heterocycles were obtained with highlights for biological applications. Synthesis, most favorable mechanism identification, *in vitro* antileishmanial potential against *L. amazonensis* and stability assays, supported by ^{125}Te NMR of a series of five- (1,2λ^4-oxatellurolanes and 1,2λ^4-benzoxatelluroles) and six- (1,2λ^4-oxatelluranes) membered ring organotelluranes, confirm products containing a Te–O bond.